PAPER

Optoelectronic characteristics of single InP nanowire grown from solid source

Materials Research Express

PAPER

Optoelectronic characteristics of single InP nanowire grown from solid source

RECEIVED
30 September 2014

REVISED
24 February 2015

ACCEPTED FOR PUBLICATION
18 March 2015

PUBLISHED
14 April 2015

H Kamimura[1], **C J Dalmaschio**[2], **S C Carrocine**[1], **A D Rodrigues**[1], **R C Gouveia**[3], **E R Leite**[4] **and A J Chiquito**[1]

[1] NanO LaB—Departamento de Física, Universidade Federal de São Carlos, CEP 13565-905, CP 676, São Carlos, São Paulo, Brasil
[2] Departamento de Ciências Naturais, Universidade Federal do Espírito Santo, CEP 29932-540, Rod. BR 101 norte, Km 60, Bairro litorâneo São Mateus, Espírito Santo, Brasil
[3] Instituto Federal de Educação, Ciência e Tecnologia de São Paulo— Campus Sertãozinho, CEP 14169-263, Rua Américo Ambrósio, 269, Jd. Canaã, Sertãozinho, São Paulo, Brasil
[4] Laboratório Interdisciplinar de Eletroquímica e Cerâmicas, Departamento de Química, Universidade Federal de São Carlos, CEP 135665-905, CP 676, São Carlos, São Paulo, Brasil

E-mail: hanay@df.ufscar.br

Keywords: nanowire, indium phosphide, photoconductivity

Abstract

InP nanowires were synthesized on quartz substrates via vapour phase deposition using gold seeds and solid source. The properties of the InP nanowires were investigated by x-ray diffraction , scanning electronic microscopy (FEG-SEM) and high resolution transmission electron microscopy demonstrating micrometric lengths and diameter distribution ranging from 40 to 100 nm with crystalline core. Photo-current on-off characteristics were obtained from single nanowire devices, presenting a delay of a few seconds in the current decay when the illumination is turned off. This time is much larger than some usual microseconds decays and may be caused by localized states whose presence was confirmed by thermally stimulated current TSC measurements.

1. Introduction

As one of the most important III–V group semiconductors, InP is an essential material for optoelectronic applications due to the direct gap of 1.35 eV at room temperature together with its high electron mobility; furthermore it is recognized as promising candidate for future applications including next generation photovoltaic cells [1–3] and other high speed electronic devices. In view of the fact that semiconductor nanostructure combines new physical properties and large surface-to-volume ratios, consequently presenting several advantages including higher photosensitivity. InP nanowires have been used for the investigation of fundamental physics in two-dimensionally such as confined nanostructures [4], single photon detectors, quantum bits [5–7].

Most of InP nanowires are grown by metal-organic vapour phase epitaxy using phosphine based phosphorus precursors [8–11]. Owing to the fact that these materials are hazardous to handle, synthesis processes using other phosphorus precursors have become considerably attractive. Liu *et al* used pieces of InP as source [12] to grow InP nanowires, with smooth surface and uniform average diameter of 100 nm along the growth direction, by vapour phase transport method in four different conditions. Strupeit *et al* synthesized InP nanoneedles by means of colloidal chemistry [13] obtaining some micrometers in length and diameter always smaller than the In seeds (below 100 nm); also, Patzke *et al* have grown InP nanowires by sublimation of InP bulk material in hydrazine atmosphere of an evacuated quartz reactor [14], achieving routes for nanowires fabrication consisting of a crystalline InP core covered by an isotropic amorphous insulator shell such as Ga and Zn.

Regardless of the fact that theses authors have made important contributions to the actual knowledge involving non-phosphine InP based nanostrucures, there are still many aspects to be investigated and potential to be explored. Achieving a route where the precursor does not present toxicity and manipulation hazards enables the nanowires fabrication in less equipped laboratories. Additionally, the practicality facilitates the fabrication of devices in large scale, such as sensors. The aim of this study is to investigate the properties of InP

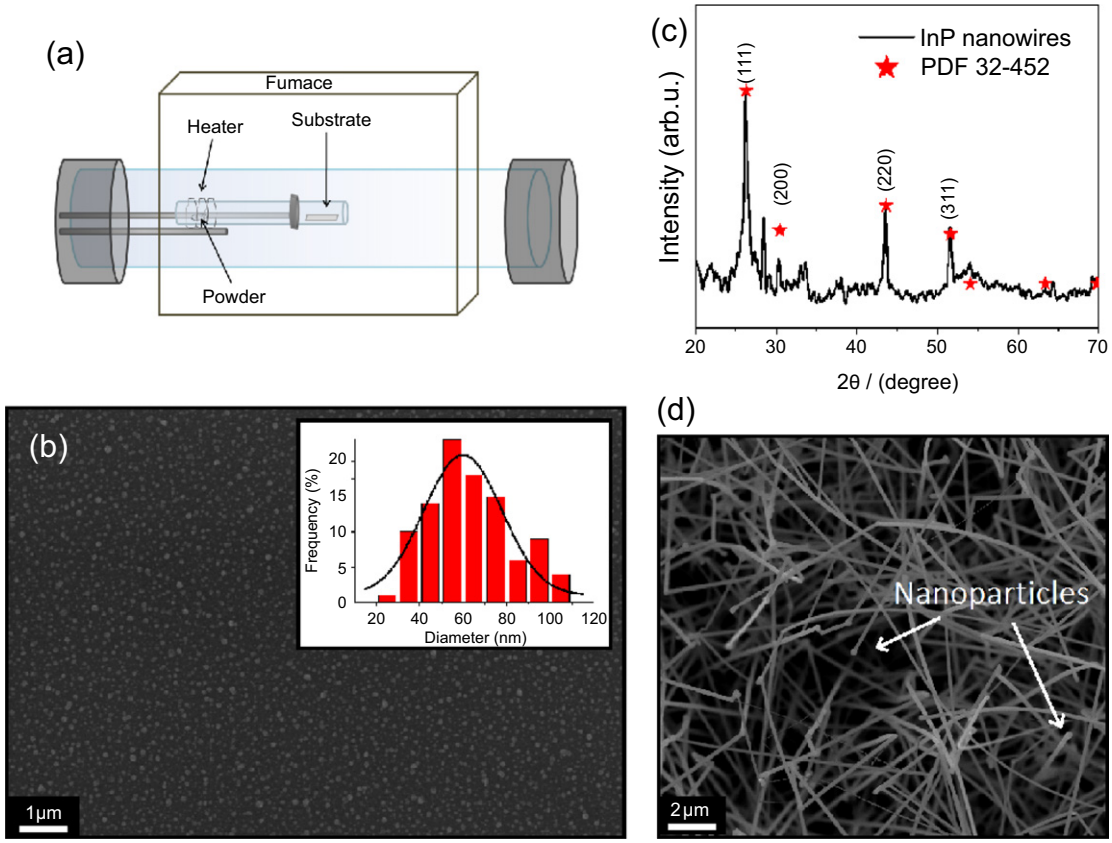

Figure 1. (a) Experimental apparatus used for the synthesis of InP nanowires. (b) Gold nanoparticles produced by thermal annealing on a substrate and the respective statistics of diameters (inset). (c) XRD pattern obtained from InP nanowires' samples, agreeing with PDF 32–542 where the cubic structure is observed. (d) FEG-SEM images of as-grown nanowires exhibiting lengths of dozens of microns and diameter ranging from 40 to 100 nm. Catalyst nanoparticles are pointed in the tips of some nanowires.

nanowires grown from InP powder precursor. For this purpose, the morphology and structure of the samples were analysed showing InP nanowires with a high quality crystalline core covered by an amorphous layer, presenting lengths of tens of micrometers and diameters ranging from 40 to 100 nm. In addition, a single nanowire device was made for the sake of exploring the potential for optoelectronic applications. For this purpose the photocurrent response was studied under laser illumination emitting in three different wavelengths, obtaining devices sensible to the visible light and allowing the extraction of spectral response and external quantum efficiency (EQE) parameters. However, these results demonstrated a current decay of a few seconds when the light was turned off, such a delay can be explained by localized states acting as traps for the carriers, whose presence was confirmed carrying out thermally stimulated current (TSC) measurements.

2. Nanowire synthesis

InP nanowires were grown by the well-known vapor-liquid-solid (VLS) mechanism [15], in which an impurity seed in liquid phase is the catalyst of the growth process, acting as a preferential site for the adsorption of vapour phase and determining nanowire dimensions [16]. Figure 1(a) depicts the experimental apparatus, where the precursor InP powder is placed inside a quartz crucible, in a region surrounded by a tungsten filament, used as heater for evaporation. Quartz substrates covered by a 2 nm thick gold layer are placed inside the same crucible, positioned in the central region of the furnace. Then, two processes are carried out for the synthesis of nanowires: fabrication of catalyst nanoparticles and nanowire growth. For the first one, the quartz substrate are annealed raising the furnace temperature to 600 °C, at pressure of 10^{-5} mbar during 15 min, resulting in a substrate uniformly covered by nanoparticles as shown in the SEM image of figure 1(b). Statistical treatments were made in the SEM images, providing diameters around 60 nm.

After this process, the furnace is cooled to the growth temperature of 450 °C, then the filament is heated to around 850 °C in order to evaporate the InP powder and an He/H_2 flux is adjusted to 20 sccm, responsible for carrying the vapour phase from the hot zone to the substrate at lower temperature, reaching a saturation state in which the vapour is adsorbed into catalysts droplets. Further adsorption causes precipitation from the droplet,

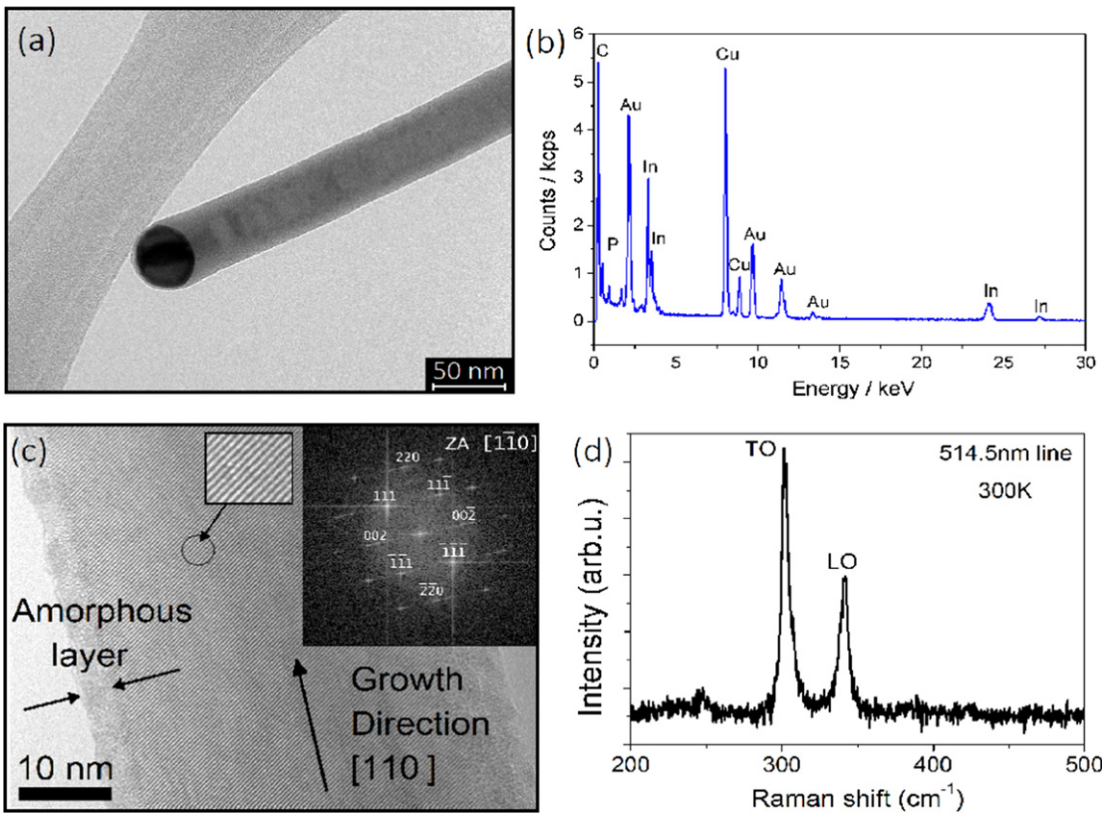

Figure 2. (a) TEM image of a nanowire's tip where the catalyst nanoparticle can be seen. In (b), the EDX analysis for the nanoparticle, composed by a Au–In alloy. The C and Cu peaks correspond to the grid used as support for the samples. (c) HRTEM image of a nanowire showing a thin amorphous layer (around 5 nm) and the growth direction (110) with a detail of the planes. In the inset, the correspondent FFT presents the distance indexed as (220), (111) and (002). (d) Raman spectrum of the nanowires, presenting peaks centred at 303 (TO phonons) and 342 cm^{-1} (LO phonons).

originating the nanowire. This conditions are kept for 1 h, then the current in the filament and the furnace are turned off, but the gas flux was maintained to avoid oxidation until the temperature decreases to 100 °C.

Scanning electron microscopy (SEM), x-ray diffraction (XRD), Raman spectroscopy were performed on the substrates just after the growth and for transmission electron microscopy (TEM), the samples were transferred to copper grids used as support.

Initially, XRD analysis were used to characterize the as-grown InP nanowires (Shimadzu, XRD 6100, 40 KV, 30 mA, Cu K radiation) and there was a remarkably match between the obtained diffraction pattern presented in figure 1(c) and the peaks from the PDF card 32–452 represented by red stars. These results indicate that the nanowires have a cubic structure and a good crystal quality with the lattice constant $a = 5.869$ Å(F–43 m space group)[5].

Figure 1(d) depicts a FEG-SEM (Zeiss Supra 35) image of the as-synthesized samples, revealing that on average, nanowires have dozens of microns in length and 40–100 nm in diameter. The diameter range obtained is comparable to the metallic nanoparticles sizes, as show in the image and histogram of the figure 1(b), in accordance with VLS growth mechanism. From TEM image, figure 2(a) the droplet presents a high phase contrast associated with the distinct atomic composition comparing nanowire and droplet. Energy-dispersive x-ray spectroscopy (EDX) spectrum from droplet region, figure 2(b), indicated the presence of Au, In and P with the respectively quantification factors, 30.47% +/−0.91, 50.96% +/−1.53 and 18.57% +/−0.58 (C and Cu signal were generated by TEM grid support).

Moreover, in figures 2(a) and (c) the high resolution transmission electron microcopy (HRTEM, Tecnai F20G2, Phillips) result shows a image for a single nanowire. In (a), there is a nanowire's tip containing the catalyst nanoparticle with the respective EDX presented in (b), indicating the droplet Au–In composition and confirming the VLS mechanism. On the other hand, it can be seen in (c) that the nanowire structure presents a crystalline core covered by a thin amorphous layer in the surface. The correspondent fast Fourier transform (inset) exhibits the distance indexed as (220), (111) and (002). The projection from ⟨110⟩ related to HRTEM image indicates a growth direction for nanowires along the (110) direction.

[5] Joint Committee on Powder Diffraction Standards (JCPDS), Card No. 32–452.

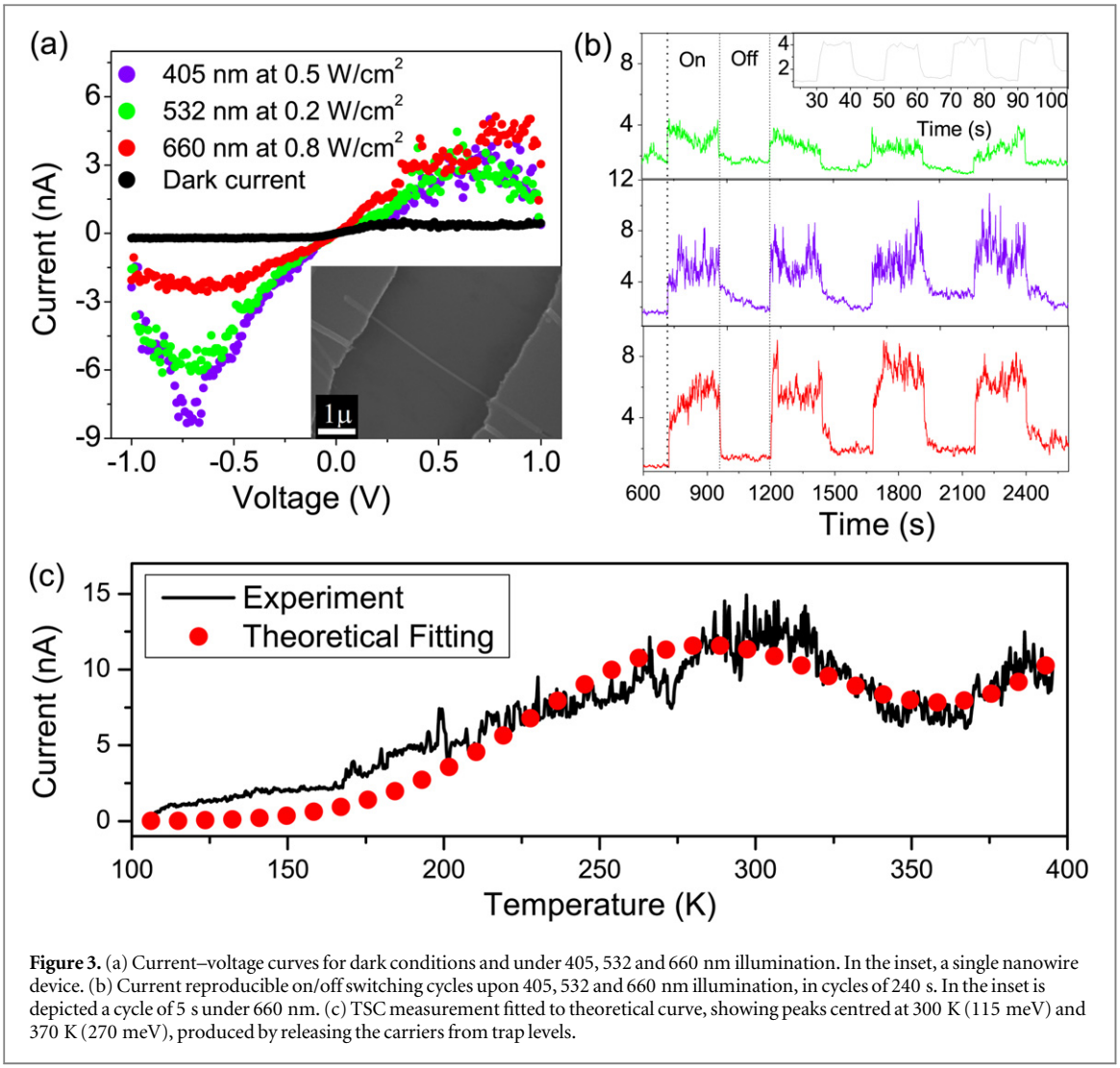

Figure 3. (a) Current–voltage curves for dark conditions and under 405, 532 and 660 nm illumination. In the inset, a single nanowire device. (b) Current reproducible on/off switching cycles upon 405, 532 and 660 nm illumination, in cycles of 240 s. In the inset is depicted a cycle of 5 s under 660 nm. (c) TSC measurement fitted to theoretical curve, showing peaks centred at 300 K (115 meV) and 370 K (270 meV), produced by releasing the carriers from trap levels.

With regard to obtain a confirmation of the previous results, Raman measurements (2(d)) were carried out using a micro Raman setup, corresponding to a spectral resolution of 1.5 cm^{-1}. The scattered light was dispersed by a triple grating monochromator and recorded by a CCD camera cooled by liquid nitrogen, using 514.5 nm line of an Ar^{+} laser as excitation. The laser power was kept lower than 1 mW so that heating could be avoided. Figure 2(d) depicts the Raman spectrum of the InP nanowires. The peaks centred at 303 and 342 cm^{-1} refer, respectively, to the transversal optical and the longitudinal optical phonons of zincblende structure of InP; moreover, the narrow peaks indicate a single crystalline core in the nanowires.

3. Device characterization

Once the samples presented interesting structural and morphological characteristics it was worth to investigate the corresponding electronic properties. In the interest of such a study, the nanowires were removed from substrate by ultrasonic agitation in ethanol solution, then dispersed on Si/SiO_2 substrates, where single nanowire devices were processed by conventional UV lithography techniques, electron beam evaporation of titanium Schottky contacts (100 nm thick) and lift-off processes, the resulting device is depicted in the inset of figure 1(a) [17].

Afterwards, *I–V* curves were obtained under dark conditions and under focused illumination (laser emitting in 660 nm, @10 mW), showing a Schottky behaviour in both cases but in the excited one there was a considerable increase in the current values, as presented in figure 3(a). Motivated by these results and aiming a investigation of the samples response to optical stimulation, the current was monitored in function of time while the device was submitted to repeated dark–light cycles under 1 V bias and 405, 532 and 660 nm illumination. The results are showed in figure 3(b), where cycles of 240 s were performed and the current values went from

Table 1. Photo response parameters for single InP nanowire based devices.

Wavelength (nm)	Spectral responsivity (R_λ)(AW^{-1})	Quantum efficiency
405	2.86	8.73
532	23.6	54.9
660	0.84	1.58

lower than 1 nA to near 4 nA for 532 nm illumination and 7 nA for 405 and 660 nm. In each curve, it is possible to notice a delay in both current increase (laser is turned on) and decrease (laser turned off).

Several devices based on multiple nanowires were made to support the findings for the three single nanowire devices, demonstrating the same behaviour in the *I–V* and photocurrent measurements, thus the data presented in this section can be considered an average result for the samples.

In the inset is depicted a cycle of 5 s in which the current increased rapidly from around 1.2 to 3.7 nA in 1 s when the red laser was turned on, and remained approximately constant between 3.5 and 3.9 nA. After 5 s the laser was turned off and the current decreased back to 1.2 nA in 3 s, being a little slower in the fall than in the rise.

Concerning photo devices, the performance can be evaluated by a critical parameter called EQE or quantum efficiency (QE), which is related to the number of electron-hole pairs excited by one absorbed photon. A high value of QE corresponds to a high sensitivity. This parameter can be expressed by [18]

$$\mathrm{QE} = \frac{hcR_\lambda}{e\lambda}, \tag{1}$$

in which R_λ is the spectral responsivity given by

$$R = \frac{\Delta I}{PS}, \tag{2}$$

where ΔI is the difference between photo-excited current and dark current, P is the light power density irradiated on the nanowire, and S is the area of nanowire and λ is the wavelength of irradiated light. Table 1 shows the parameters for the single nanowire devices under illumination of lasers emitting in 405 (at 0.5 W cm^{-2}), 532 (at 0.2 W cm^{-2}) and 660 nm (at 0.8 W cm^{-2}), where the distance between the electrodes is 5 μm and the nanowires length are 100 nm. The devices exhibited photo-current response at the three different wavelengths used, allowing the extraction of some important optical parameters.

The delay in photo-response for both the rising and falling photo-current can be caused by the presence of carrier trap states originated from disorder present in the structure. Such disorder can be originated from the self-organizing growth mechanism and from the crystalline/amorphous interface.

On account of verifying the presence of these trapping states, TSC measurements (TSC) were performed in a closed cycle helium cryostat (Janis Research, CCS 400 H) at pressures below 10^{-6} T. The current was monitored by an electrometer (Keithley Instruments, 6517B). In this procedure, the sample was irradiated with red laser (660 nm) and cooled to 100 K, thus stimulating carriers trapped in deep levels lying in the forbidden energy gap. If there is a electron trapping centre with energy above the normal dark Fermi level, then trapped electrons will be in a non-equilibrium state, thereby their rate of release will depend mainly on the phonon energy available in the lattice [19]. Thus, after removing the optical stimulation the traps will empty into the conduction band with the rise of temperature, producing temporary increases in the electric current. As the number of filled traps diminishes with time and there is no injection due to the Schottky barrier, the excess conductivity presents maximum points. In the case of the samples, peaks were observed to be centred around 300 and 370 K, as showed in figure 3(c). These data were adjusted to the equation [20]

$$I_{\mathrm{TSC}}(T) = I_0 N_{C,V} \exp\left(-\frac{\Delta E}{k_B T} - \frac{1}{N_T \beta \tau} \times \int_{T_0}^{T} N_{C,V} \exp\left(-\frac{\Delta E}{k_B T}\right) \mathrm{d}T\right), \tag{3}$$

where I_0 is related to the trap properties, $N_{C,V}$ is the number of carriers at the conduction (valence) band, τ is the carrier lifetime, N_T is the number of traps, ΔE is the activation energy necessary to release trapped carriers, T_0 is the trap filling temperature and β is the heating rate used in the experiment. The red curve in figure 3(c) represents the fitting to this model with a remarkable agreement between theoretical and experimental points in the whole range of temperature (100 K $< T <$ 400 K), showing the presence of additional levels around 115 and 270 $\pm$ 10 meV. Hole trap activation energies of 120 and 270 meV was reported for bulk InP and was associated to

native defects in crystal lattice, such as vacancies [21, 22]. The observed delay can be caused by these levels that capture carriers and then release them back to the band from which they were captured, thus the carrier is temporarily trapped onto a level instead of recombining directly [23].

4. Conclusion

To summarize, the development of a procedure simplier, considerably less hazardous and more economic than common phosphine-based methods for InP nanowires synthesis was accomplished, using gold seeds for vapour phase deposition from solid source. Produced nanowires presented highly crystalline core with dozens of microns in length and diameter distribution ranging from 40 to 100 nm. The quality of the samples is comparable to the usual and alternative routes of synthesis and the plenty of nanowires in the substrates make interesting the use of this route for devices readily made and in large scale, such as sensors. Aiming these applications, photocurrent measurements on single InP nanowire devices built using Ti electrodes showed that the sample responds to different wavelength in the range of visible light (405, 532 and 660 nm). Under successive light–dark cycles, the samples presented a delay in photoresponse, which may be explained by the presence of localized states. In order to investigate this phenomenon, TSC measurements were carried out and indicated the presence of energy states at 110 and 270 meV. These results agree with the obtained data from HRTEM and photocurrent curves indicating that native structural defects from the self-organizing growth mechanism and from the crystalline/amorphous interface generate trapping centres which affect the photocurrent behaviour.

Acknowledgments

The authors thank the Brazilian research funding agencies FAPESP (2012/06916-4) and CNPq (302640/2010-0, 471086/2013-4) for the financial support of this work.

References

[1] Dick K A 2008 *Prog. Cryst. Growth Charact. Mater.* **54** 138
[2] Kayes B M, Atwater H A and Lewis N S J 2005 *Appl. Phys.* **97** 114302
[3] Heurlin M, Wickert P, Fält S, Borgström M T, Deppert K, Samuelson L and Magnusson M H 2011 *Nano Lett.* **11** 2028
[4] Yu H, Li J, Loomis R, Wang L W and Buhro W E 2003 *Nat. Mater.* **2** 517
[5] Nadj-Perge S, Frolov S M, Bakkers E P A M and Kouwenhoven L P 2010 *Nature* **468** 1084
[6] Hu Y, Kuemmeth F, Lieber C M and Marcus C M 2012 *Nat. Nanotechnology* **7** 47
[7] Agarwal R 2008 *Small* **4** 1872
[8] Wallentin J, Ek M, Wallenberg L R, Samuelson L and Borgström M T 2012 *Nano Lett.* **12** 151
[9] Mohan P, Motohisa J and Fukui T 2006 *Appl. Phys. Lett.* **88** 133105
[10] Vu T T T, Zehender T, Verheijen M A, Plissard S R, Immink G W G, Haverkort J E M and Bakkers E P A M 2013 *Nanotechnology* **24** 115705
[11] Bhunia S, Kawamura T, Fujikawa S, Nakashima H, Furukawa K, Torimitsu K and Watanabe Y 2004 *Thin Solid Films* **464** 244
[12] Liu C, Dai L, You L P, Xu W J and Qin G G 2008 *Nanotechnology* **19** 465203
[13] Strupeit T, Klinke C, Kornowski A and Weller H 2009 *ACS Nano* **3** 668
[14] Patzke G R, Kontic R, Shiolashvili Z, Makhatadze N and Jishiashvili D 2013 *Materials* **6** 85
[15] Wagner R S and Ellis W C 1964 *Appl. Phys. Lett.* **4** 89
[16] Cao G 2004 *Nanostructures and Nanomaterials: Synthesis, Properties and Applications* (London: Imperial College Press)
[17] Razeghi M 2010 *Technology of Quantum Devices* (New York: Springer)
[18] Sze S M 1981 *Physics of Semiconductor Devices* (New Jersey: Wiley)
[19] Wright H C and Allen G A 1966 *Br. J. Appl. Phys.* **17** 1181
[20] Berengue O M, Kanashiro M K, Chiquito A J, Dalmaschio C J and Leite E R 2012 *Semicond. Sci. Technol.* **27** 065021
[21] Choudhury A N M M and Robson P N 1979 *Electron. Lett.* **15** 247
[22] Hu B H, Zhou B L and Chen Z X 1988 *J. Lumin.* **40** 371
[23] Schroder D K 2006 *Semiconductor Material and Device Characterization* 3rd edn (New Jersey: Wiley)